

Computational Evaluation on the Use of Some Selected Ceramic MAX-Phase Coatings as Shielding Layers on Spent Fuel Dry Cask Canisters

Zeinab Y. Alsmadi^{1*}, Mohamed A. Bourham¹

¹Department of Nuclear Engineering, North Carolina State University, Raleigh, NC 27695-7909

Abstract

The gamma-ray shielding properties of some MAX-phase titanium carbide ceramic materials were computationally investigated, as potential coating layers on the canisters in spent fuel dry storage casks using MicroShield software package. It was observed that titanium silicon carbide Ti_3SiC_2 exhibited the highest linear and mass attenuation coefficients, lowest half-value layer (HVL) and mean-free path (MFP) values, while titanium aluminum carbide Ti_2AlC showed the highest rate of exposure to gamma radiation and Ti_3SiC_2 showed the lowest rate. The MAX-phase titanium carbide with silicon has higher molar mass and provides higher mass attenuation coefficient than the one with aluminum inclusion. Coating the outer wall of the canister with a thin layer of MAX-phase titanium carbide material can provide additional shielding and a diffusion barrier, which enhances the performance of the high-level spent fuel storage in dry casks.

Keyword

Shielding properties; MAX-phase; Canister coating; Dry cask; MicroShield

Date of Submission: 05-01-2023

Date of Acceptance: 19-01-2023

I. Introduction

In radiation shielding, the shield typically placed between the radiation source and the protected object and/or human being, and is applied using various forms of materials such as multilayer shielding materials, composite shields or a combination of both. Composite shielding materials are mainly composed of a base material mixed with other additives and aggregates, as usually the case for concrete and mortars, and is composed of multilayer shielding layers of different materials to allow scattered and absorbed radiation within the layers [1-5]. Choosing the type of shield configuration depends on the application in which radiation shielding materials have different shielding properties that can be mixed and developed to provide a specific shielding [1-2].

Spent fuel from nuclear power plants stored in dry casks emit high-levels of radiation and hence, dry casks must provide excellent shielding to encase radiation within the cask without radiation leaking out to the environment. Dry casks are composed of stainless-steel canisters enclosing the spent fuel, and may have glass-based or ceramic coatings followed by a heavy concrete overpack with an airgap between the canister and the overpack [6-9]. These coatings provide shielding and barriers for diffusion, thermal stability against high-levels radiation, as well as temperatures and corrosive environments [1, 2, 5, 10]. Ceramic coatings developed with excellent corrosion resistance, neutron absorption and economic feasibility for various applications in spent fuel storage systems, waste packages, drip shield in repositories and naval vessels [11].

A family of layered compounds in the Ti-Al-C-N system with a chemical formula $M_{n+1}AX_n$ where $n=1,2,3$ and M is an early transition metal, A is a group element, and X is carbon or nitrogen, have been developed in the state between metal and ceramic properties [12-17].

They are known as Hägg-phases, H-phase, Novotny-phases, thermodynamically stable nanolaminates or MAX-phase materials. This type of materials has shown a unique set of properties due to their atomic bonding and structural characteristics, such as good thermal and electrical conductivity, low thermal expansion coefficient, damage tolerance and some are oxidation, creep, fatigue and creep-fatigue resistant such as Ti_2AlC and Ti_3SiC_2 [13-31]. They are employed in many applications such as heating elements, nozzles, patrol vehicles, helicopters, heat exchangers and cladding materials in nuclear reactors [12, 14-16, 28, 32, 33]. However, as there have been a lot of studies conducted to study the mechanical, thermal and electrical properties of MAX-phase materials for various applications as mentioned earlier, no studies were conducted to investigate their shielding properties as spent fuel dry cask canisters coatings as nuclear energy progresses.

In this paper, the shielding properties of three MAX-phase materials: titanium silicon carbide Ti_3SiC_2 , and two titanium aluminum carbides Ti_2AlC and Ti_3AlC_2 are investigated as new canister coatings in spent fuel

dry storage casks using the MicroShield[®] computational software. In this study, the model of a dry cask consists of three layers. These are an inner layer of the Alloy 709 advanced austenitic stainless-steel canister from the work of Alsmadi et al. [2], an intermediate shielding coating of MAX-phase materials, which is the purpose of this study and an outer shielding layer of concrete overpack known as ‘Concrete 6’ from the work of Waly et al. [34].

II. Materials and Methods

2.1 Materials

The canister coating materials investigated in this work belong to a family of layered compounds known as MAX-Phase materials such as Ti₃SiC₂, Ti₃AlC₂ and Ti₂AlC, in which they are the most common MAX-phases synthesized. Table 1 depicts their chemical composition and density while Table 2 depicts some of their mechanical properties [13]. The most common MAX-phase material for high-temperature applications is Ti₂AlC due to its superb oxidation resistance and cheap cost among other MAX-phases [14, 15]. As mentioned above, these materials have highly anisotropic properties laying between metals and ceramics. They exhibit high elastic modulus, high electrical and heat conductivity, low hardness and very high fracture toughness [16]. Moreover, MAX-phase materials are elastically stiff, resistant to chemical attack and thermal shock, relatively soft and readily machinable. One of the most important properties of MAX-phases is their temperature limitation in which they tend to dissociate at high temperatures under high vacuum conditions. Given the remarkable and unique set of properties of MAX-phase materials, they have become attractive for many applications such as rotating electrical contacts and bearings, tools for die pressing, heating elements, heat exchangers, cladding materials in nuclear power plants and many more [12-16, 28, 32, 33].

Alloy 709 (Fe-25Ni-20Cr) advanced austenitic stainless steel has proven to have the highest attenuation against gamma radiation, as a dry cask canister material compared to other stainless steels such as 304, 316 and 303Cu stainless steels, due to its high weight fraction of chromium (Cr), nickel (Ni) and other additives of niobium (Nb), titanium (Ti) and boron (B)[2]. The chemical composition of the Alloy 709 is shown in Table 3. On the other hand, Waly et al [34] performed an investigation on the shielding properties of different concrete overpack as the outer shielding layer of the dry cask, and concluded that ‘Concrete 6’ with the chemical composition and density presented in Table 4, has the highest attenuation and lowest exposure rate compared to ordinary concrete.

The H. B. Robinson spent fuel [34,35] is used in this research as the model of the spent fuel source with depletion of 72 GWd/MTU burnup 8-year decay.

Table 1. Chemical composition (wt%) and density of MAX-phase materials.

Material	Density (g/cc)	Ti	C	Al	Si
Ti ₂ AlC	4.1	71.06	8.91	20.02	-
Ti ₃ AlC ₂	4.24	73.79	12.34	13.86	-
Ti ₃ SiC ₂	4.5	73.38	12.27	-	14.34

Table 2. Mechanical properties of MAX-phase materials [13].

Material	Young’s Modulus, E (GPa)	Shear Modulus, G (GPa)	Fracture Toughness, K _{Ic} (MPam ^{1/2})
Ti ₂ AlC	277	118	6.5
Ti ₃ AlC ₂	297	124	6.9-9.5
Ti ₃ SiC ₂	340-347	139	7-16

Table 3. Chemical composition (wt%) of the Alloy 709 [2].

Element	Fe	Ni	Cr	Mo	Mn	Si	Nb	N	C	Ti	P	B	S
Wt%	Bal.	24.98	19.93	1.51	0.91	0.44	0.26	0.148	0.07	0.04	<0.014	0.0045	<0.001

Table 4. Chemical composition (wt%) and density of Concrete 6 [2, 34].

Material	Density (g/cc)	CaO	SiO ₂	Al ₂ O ₃	Fe ₂ O ₃	MgO	SO ₃	Na ₂ O	K ₂ O	H ₂ O	CaCO ₃	Fe ₃ O ₄	PbO
Concrete 6	4.64	8.8074	21.8892	0.4194	0.699	0.4194	0.4194	0.04194	0.09786	7.63	4.7034	39.195	15.678

2.2 Computational Methods

MicroShield® v9.05 (MSD9) software [36] is used in this work to study the shielding properties of MAX-phase materials, such as linear and mass attenuation coefficients, half-value layer (HVL), the exposure rates, mean free path (MFP) and exposure buildup factor. MicroShield is a deterministic code; however, it produces results similar to MCNP, which is a Monte Carlo code, and other photon transport packages. MicroShield® provides a large set of configurations for the source geometry. The performance of the computational simulation using this software package requires the geometry of the dry cask along with spent fuel source and shielding layers dimensions and density, and the spent fuel isotopic composition. MicroShield® is approved by the US Nuclear regulatory Commission (NRC) and is widely used by researchers to design shields and estimate their exposure to gamma radiation [37-41]. As shown in Fig.1, the 8.727 ft radius and 20 ft high cylindrical spent fuel source is surrounded by 0.27 ft thick cylindrical Alloy 709 canister, 0.2 ft thick cylindrical MAX-phase coating, 0.167 ft thick air gap for heat removal and 1.8 ft thick cylindrical concrete overpack. The dose point is located on the dry cask outer surface and is 10 ft away from the source.

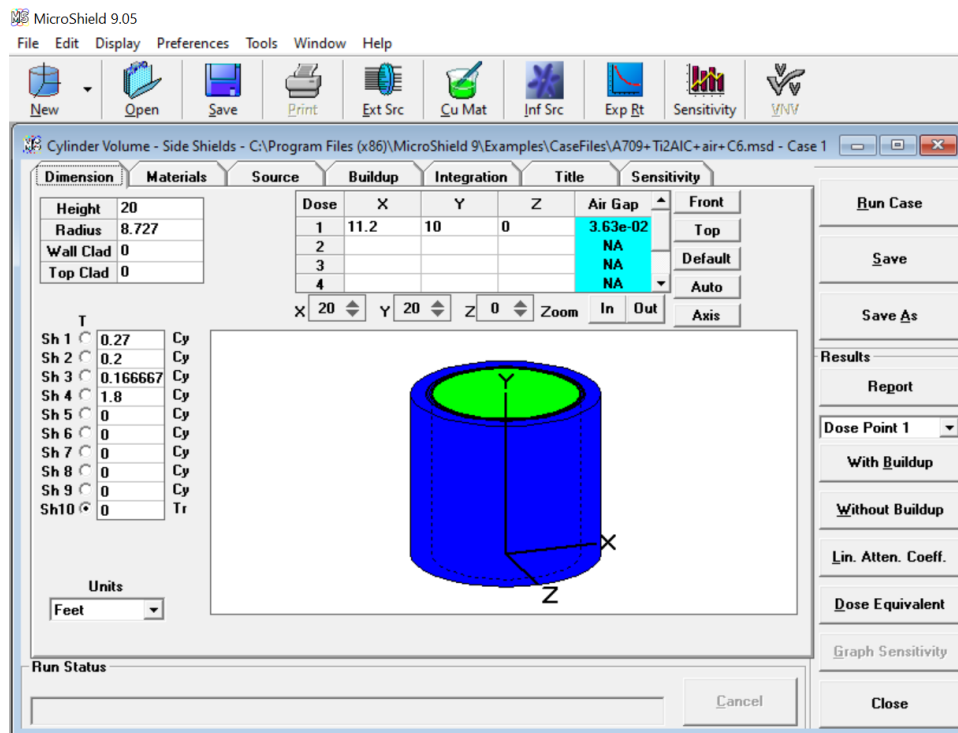


Fig. 1. The spent fuel dry cask computational setup using MicroShield® with MAX-phase materials as canister coating.

III. Results and Discussion

3.1 Linear and Mass Attenuation Coefficients

The linear attenuation coefficient, μ , is the interaction probability of gamma radiation with target material per unit path length and is expressed in cm^{-1} , while the mass attenuation coefficient, μ/ρ , is the interaction probability of gamma radiation with target material per unit mass and is expressed in cm^2/g . Both parameters are important to study in any shielding assessment, as they describe the efficiency of shielding material in attenuating gamma radiation of incident intensity, I_0 . The transmitted intensity, I , by the shielding material of thickness, x , is given as following [2, 42]:

$$I = I_0 e^{-\mu x} \quad (1)$$

Fig. 2 shows the linear attenuation coefficient for the three selected MAX-phase materials as function of photon energy while Fig. 3 shows the mass attenuation coefficient. Although slightly differs from each other, however, as shown, the Ti_3SiC_2 has the highest linear and mass attenuation coefficients compared to other MAX-phases at all photon energies ranging from 0.015 MeV to 3.0 MeV, while Ti_2AlC has the lowest attenuation coefficients values and Ti_3AlC_2 falls in between. The linear and mass attenuation coefficients values are also shown in Table 5 and Table 6. The difference in the attenuation values becomes smaller with increasing photon energies. The high gamma-ray attenuation values of Ti_3SiC_2 can be related to its high density of 4.5 g/cm^3 and its silicon (Si) content, which has a higher molar mass (28.0855 g/mol) than aluminum (Al) (26.9815

g/mol) included in other MAX-phases and therefore, the increasing density will indicate higher probability of interacting with the incident photons and thus higher gamma-rays attenuation, which enhances the shielding efficiency of Ti_3SiC_2 against gamma radiation at all photon energies.

Fig. 4 and Table 7 show a comparison of the summation of linear attenuation coefficients of the spent fuel dry cask canister and heavy concrete overpack, with and without selected MAX-Phase coatings. As shown, the linear attenuation coefficient of the dry cask increases when the Alloy 709 canister is coated with MAX-phase materials, where the difference in the linear attenuation coefficient values increases with increasing photon energy (Fig. 4(a)). Furthermore, the shielding efficiency of the dry cask enhances significantly when the Alloy 709 canister is coated with Ti_3SiC_2 , especially at high energies, in which Ti_3SiC_2 exhibits the highest attenuation coefficient values compared to other MAX-phase coatings due to its high density and Si content (Fig. 4(b)).

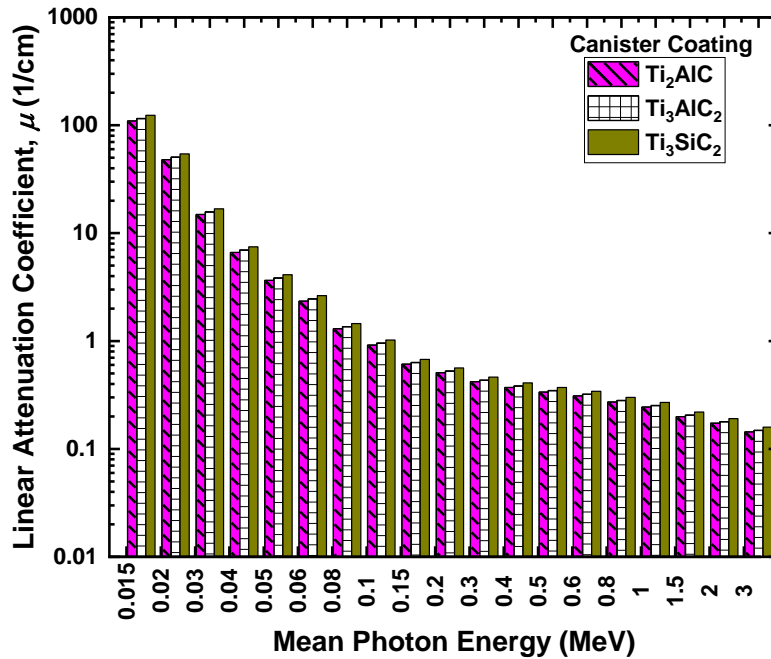


Fig. 2. Linear attenuation coefficient as function of photon energy for the selected MAX-phase materials.

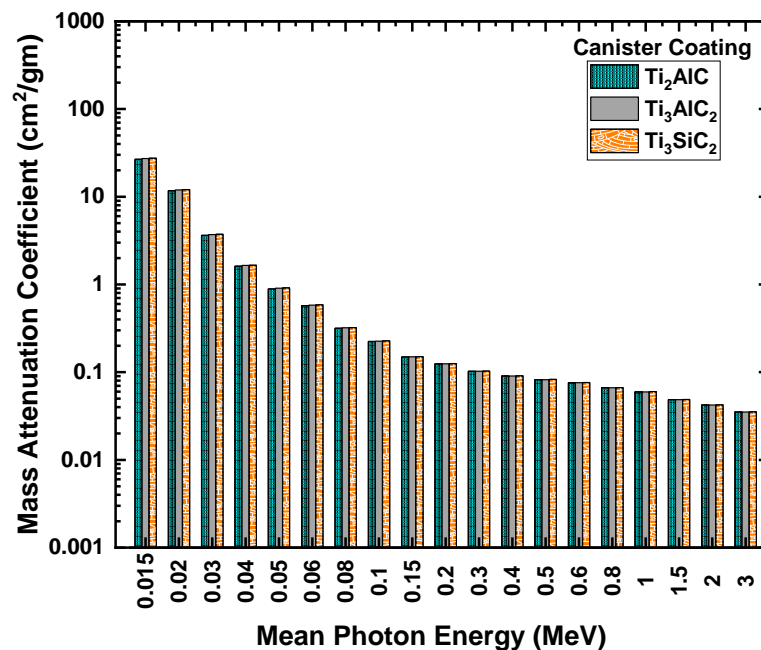


Fig. 3. Mass attenuation coefficient as function of photon energy for the selected MAX-phase materials.

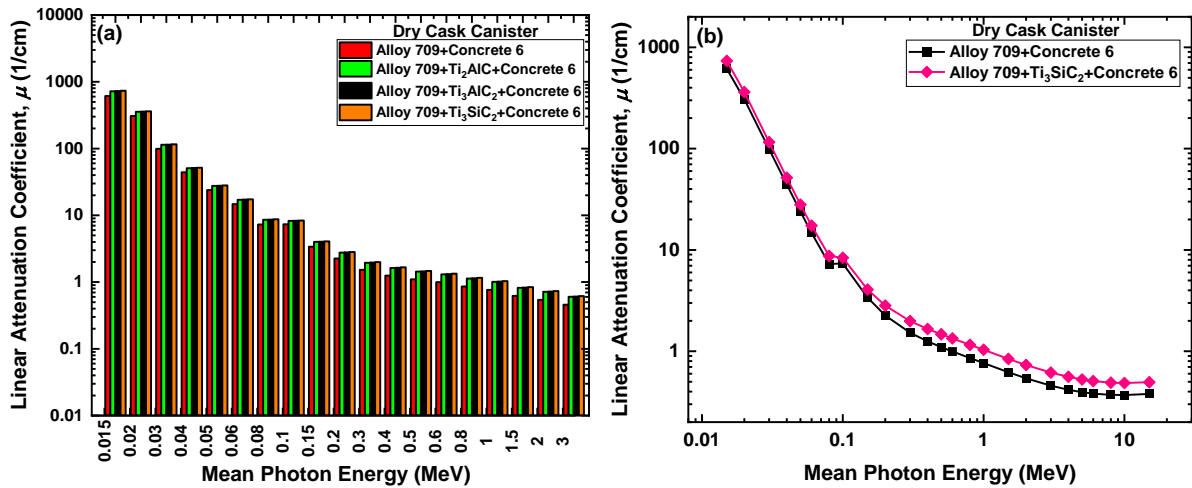


Fig. 4. Comparison of linear attenuation coefficient of the dry cask with and without selected MAX-Phase coatings (a) and the same comparison with and without Ti_3SiC_2 MAX-phase coating at different photon energies (b).

Table 5. Linear attenuation coefficient of MAX-phase materials at different photon energies.

Energy (MeV)	Ti_2AlC (cm^{-1})	Ti_3AlC_2 (cm^{-1})	Ti_3SiC_2 (cm^{-1})
0.015	109.6	115.5	123.6
0.02	48	50.64	54.17
0.03	14.9	15.72	16.81
0.04	6.619	6.981	7.461
0.05	3.653	3.848	4.111
0.06	2.342	2.463	2.631
0.08	1.298	1.359	1.451
0.1	0.9178	0.9577	1.022
0.15	0.6106	0.6339	0.6764
0.2	0.5097	0.5281	0.5635
0.3	0.4198	0.4344	0.4635
0.4	0.3708	0.3835	0.4092
0.5	0.3367	0.3482	0.3715
0.6	0.3105	0.3212	0.3427
0.8	0.2721	0.2814	0.3003
1.0	0.2444	0.2527	0.2696
1.5	0.1993	0.2061	0.2199
2.0	0.1731	0.179	0.191
3.0	0.144	0.1489	0.159

Table 6. Mass attenuation coefficient of MAX-phase materials at different photon energies.

Energy (MeV)	Ti_2AlC (cm^2/g)	Ti_3AlC_2 (cm^2/g)	Ti_3SiC_2 (cm^2/g)
0.015	26.7288	27.24627	27.47211
0.02	11.70738	11.94278	12.03679
0.03	3.63358	3.7082	3.73549
0.04	1.61432	1.64651	1.65795
0.05	0.891	0.9076	0.91364
0.06	0.57131	0.58092	0.58464
0.08	0.31649	0.3205	0.32241
0.1	0.22385	0.22588	0.22717
0.15	0.14892	0.1495	0.15031
0.2	0.12431	0.12455	0.12521
0.3	0.10239	0.10246	0.10301
0.4	0.09043	0.09046	0.09094
0.5	0.08211	0.08213	0.08256
0.6	0.07574	0.07575	0.07615
0.8	0.06637	0.06638	0.06673

1.0	0.0596	0.05961	0.05992
1.5	0.04861	0.04861	0.04887
2.0	0.04221	0.04221	0.04244
3.0	0.03513	0.03513	0.03533

Table 7. Comparison of linear attenuation coefficient of the dry cask canister with and without MAX-Phase coatings at different photon energies.

Energy (MeV)	Alloy 709+Concrete 6 (cm ⁻¹)	Alloy 709+Ti ₂ AlC+Concrete 6 (cm ⁻¹)	Alloy 709+Ti ₃ AlC ₂ +Concrete 6 (cm ⁻¹)	Alloy 709+Ti ₃ SiC ₂ +Concrete 6 (cm ⁻¹)
0.015	612.5	722.1	728	736.1
0.02	307.34	355.34	357.98	361.51
0.03	98.95	113.85	114.67	115.76
0.04	44.21	50.829	51.191	51.671
0.05	23.912	27.565	27.76	28.023
0.06	14.739	17.081	17.202	17.37
0.08	7.276	8.574	8.635	8.727
0.1	7.345	8.2628	8.3027	8.367
0.15	3.392	4.0026	4.0259	4.0684
0.2	2.26	2.7697	2.7881	2.8235
0.3	1.5259	1.9457	1.9603	1.9894
0.4	1.2517	1.6225	1.6352	1.6609
0.5	1.0992	1.4359	1.4474	1.4707
0.6	0.9966	1.3071	1.3178	1.3393
0.8	0.8585	1.1306	1.1399	1.1588
1.0	0.765	1.0094	1.0177	1.0346
1.5	0.6208	0.8201	0.8269	0.8407
2.0	0.5415	0.7146	0.7205	0.7325
3.0	0.4582	0.6022	0.6071	0.6172

In comparison to an attempt of using MAX-phase materials as protective shielding coatings on spent fuel dry cask stainless-steel canisters, lead oxide glass (PbO) is used as an intermediate shielding layer on the dry cask canisters due to their high density and thermal stability [2, 6, 43]. Waly et al. [42] investigated six different types of glass systems as gamma radiation shields materials with different chemical compositions using MicroShield® in the energy range 0.015-15 MeV, and found that the inclusion of PbO and Bi₂O₃ enhances the shielding properties against gamma radiation. Among those different compositions studied, the composition named as “Glass 6” has shown to have the highest mass attenuation coefficient and the smallest HVL compared to other compositions, with the chemical composition and density represented in Table 8.

Table 8. Chemical composition (wt%) and density of Glass 6 [2, 6, 42].

Material	Density (g/cc)	PbO	Al ₂ O ₃	SiO ₂
Glass 6	8.284	80	10	10

Fig. 5 shows the comparison of linear attenuation coefficient between different MAX-phase materials and Glass 6 at photon energies ranging from 0.015-3.0 MeV. As shown, Glass 6 exhibits higher attenuation coefficient values than all MAX-phases investigated here due to its high density of 8.284 g/cm³ compared to the much lower density of all MAX-phases. Also, Glass 6 attenuation values decrease with increasing photon energy except at about 0.09 MeV, in which it increases below the absorbing K-edge that corresponds to the binding energy of an electron K-shell. However, while Glass 6 exhibits better attenuation than MAX-phases, MAX-phase materials have better mechanical and thermal properties than Glass 6.

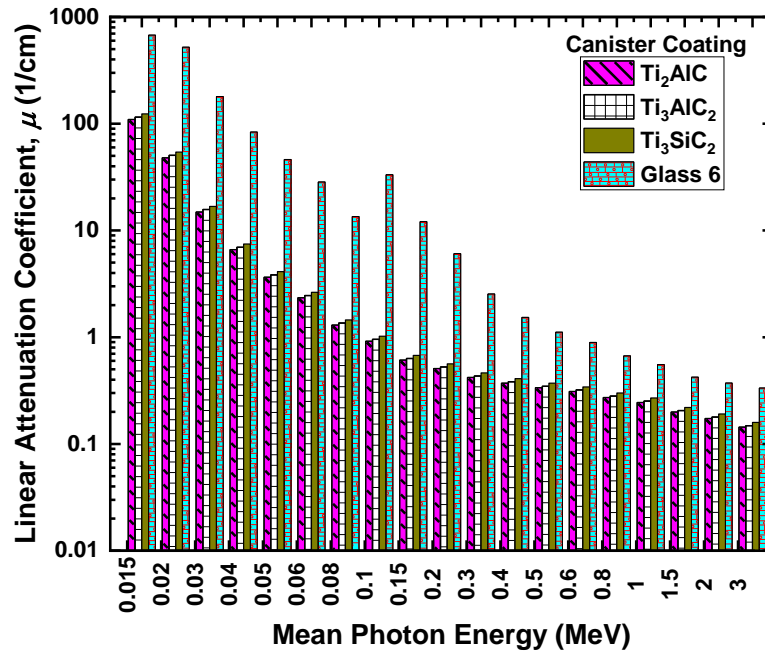


Fig. 5. Comparison of linear attenuation coefficient between MAX-phase materials and Glass 6.

3.2 Half Value Layer and Mean Free Path

The thickness of the material in which the incident radiation density is reduced by half is known as the half-value layer (HVL) and it is $\ln(2)/\mu$, which means that the better shielding attenuation, the lower the value of the HVL. On the other hand, the average distance gamma-rays travel in the target shielding material before interacting is called mean free path (MFP), and it is expressed as $1/\mu$ [2]. The HVL values obtained from MicroShield[®] for the different MAX-phase materials as function of photon energy are shown in Fig. 6 and the incident gamma radiation MFP values are shown in Fig. 7. As represented in Fig. 6, values of the HVL increase with increasing photon energy in which Ti_2AlC exhibits the highest HVL at photon energies ranging from 0.03 – 15 MeV. At 0.015 – 0.02 MeV, HVL values are somehow similar between all MAX-phases. The lowest HVL is attributed to Ti_3SiC_2 due to its high density of 4.5 g/cm^3 and its silicon (Si) content, which has a higher molar mass (28.0855 g/mol) than aluminum (Al) (26.9815 g/mol) included in other MAX-phases. Similarly, Ti_3SiC_2 represents the lowest MFP values as shown in Fig. 7, followed by Ti_3AlC_2 and then Ti_2AlC which exhibits the highest MFP values.

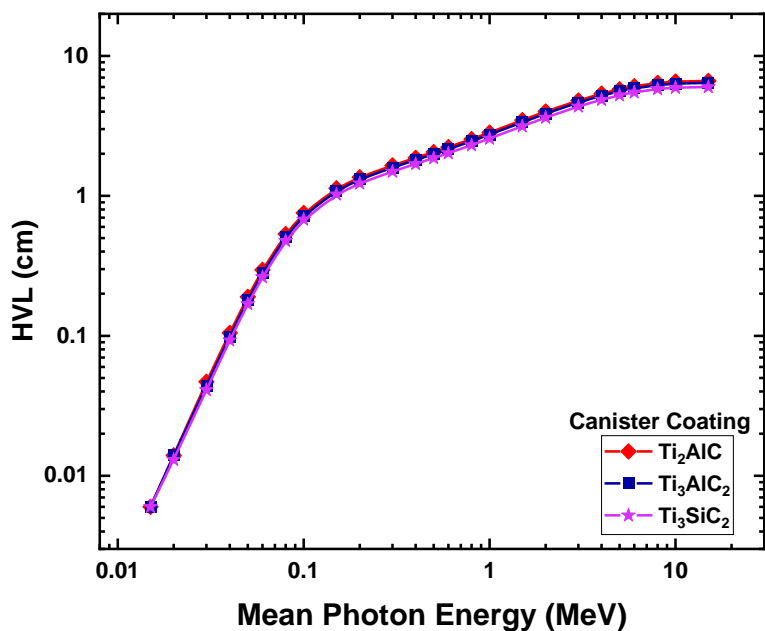


Fig. 6. Half-value layer (HVL) values as function of photon energy for different MAX-phases.

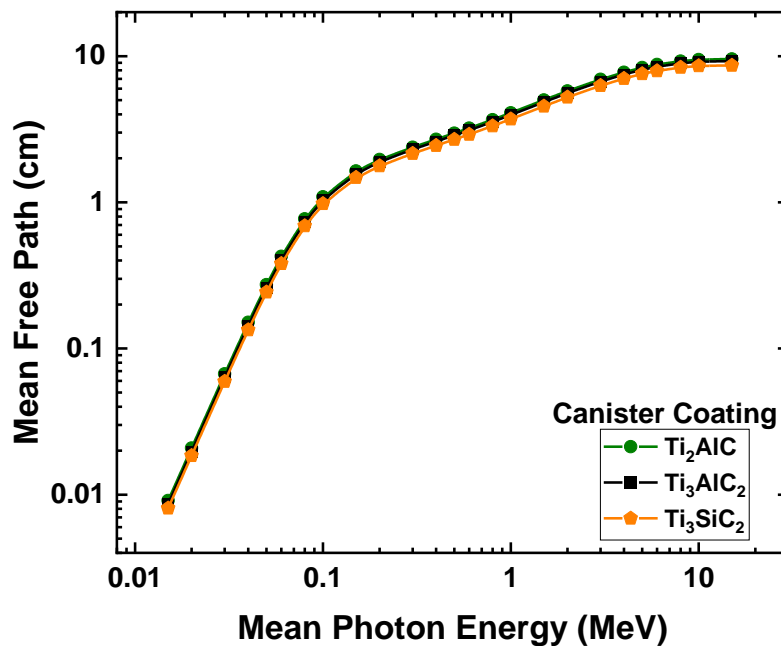


Fig. 7. Mean free path (MFP) values as function of photon energy for different MAX-phases.

3.3 Exposure Rate

Fig. 8(a) shows the exposure rate with no build up in mR/hr calculated at the outer spent fuel dry cask canister surface, for different canister coatings of MAX-phase materials along with the concrete overpack, in which the exposure rate increases with photon energy to reach its highest value of $6.879E-7$ mR/hr at 1.5 MeV for Ti₂AlC then it starts to decrease again. The exposure rates below 0.3 MeV mean photon energy are not represented since they are negligible. On the other hand, Fig. 8(b) shows the exposure rate with buildup in which buildup is observed to influence the exposure rate at low photon energies with a significant difference between different MAX- phases, whereas this difference decreases with increasing photon energy up to 4 MeV. At low photon energies, Ti₂AlC dry cask coating shows a much higher exposure rates values compared to other MAX-phases, while Ti₃SiC₂ shows the lowest rates of exposure to ionizing radiation when used as dry cask canister coating. Also, Ti₃SiC₂ coating keeps to show the lowest values of exposure rates at high photon energies due to its high density of 4.5 g/cm^3 and its silicon (Si) content. Moreover, the MAX-phase coating that shows the highest rate of exposure to gamma radiation at 1.5 MeV is Ti₂AlC, with an exposure rate of $3.216E-5$ mR/hr compared to the other two MAX-phases.

To compare the exposure rate values of MAX-phase materials with one of the most common glass systems with high attenuation coefficients and low exposure rates, Fig. 9 shows the exposure rate (with buildup) at the outer spent fuel dry cask surface for different MAX-phases, compared to Glass 6 along with the concrete overpack in both systems. As show, Glass 6 exhibits lower exposure rates than all MAX-phase materials, due to its high density compared to MAX-phases. which is similar to what is observed in Fig. 5.

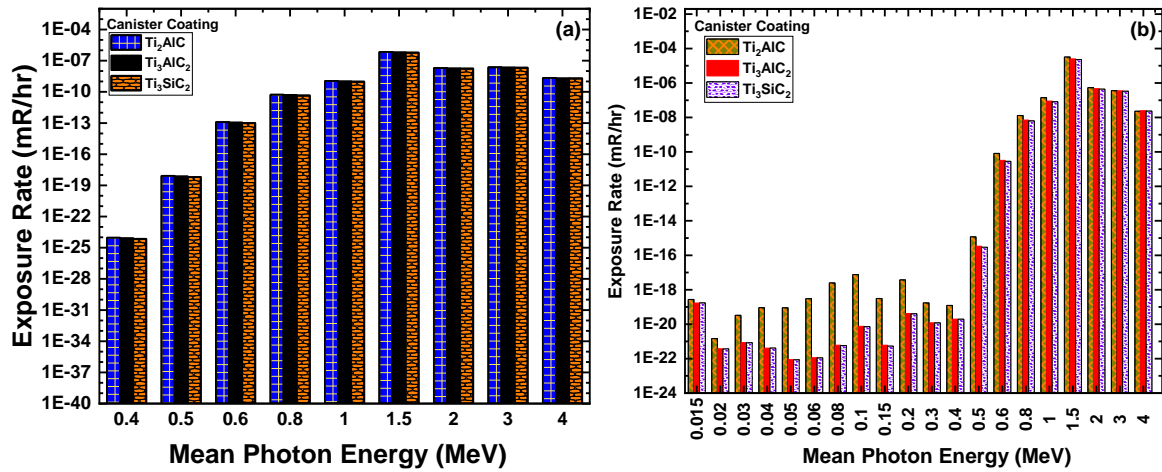


Fig. 8. Exposure rate at the outer spent fuel dry cask canister coated surface for the selected MAX-phases along with the concrete overpack with no buildup (a) and with buildup (b).

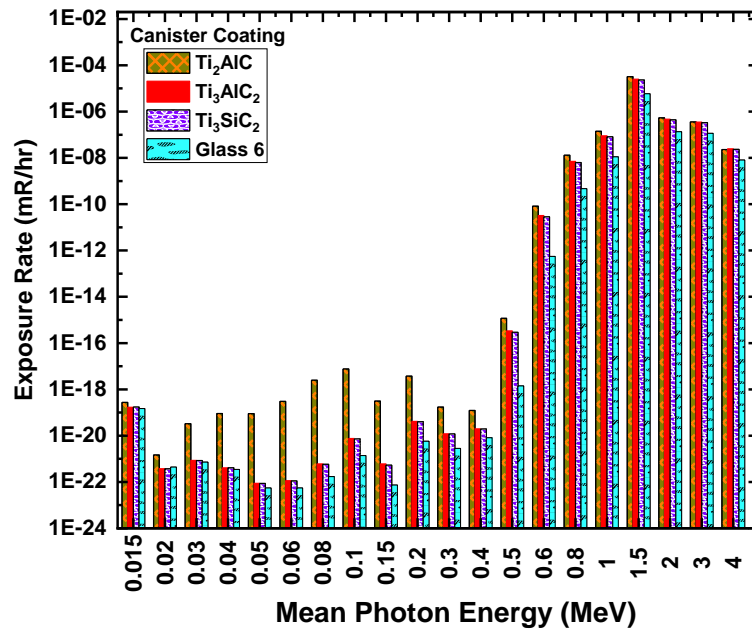


Fig. 9. Comparison of exposure rate (with buildup) values at the outer spent fuel dry cask surface for the selected MAX-phases and Glass 6 along with the concrete overpack in both systems.

3.4 Exposure Buildup Factor

The variation of exposure buildup factor as function of mean photon energy is shown in Fig. 10, at fixed penetration depth of 20 MFP. As shown, this variation is attributed to the three types of gamma interaction with matter; Photoelectric effect that results in increasing the exposure buildup at low energies, Compton scattering that results in the highest exposure buildup at intermediate energies and Pair production that results in decreasing the exposure buildup values at high energies [34, 42]. Among all MAX-phases investigated, Ti_3SiC_2 canister coating exhibits the lowest values of exposure buildup at photon energies ranging from 0.015 – 2.0 MeV, while Ti_2AlC and Ti_3AlC_2 coatings exhibit the lowest buildup values at energies ranging from 3.0 – 15 MeV. Furthermore, Fig. 11 shows the variation of exposure buildup values at fixed photon energy of 10 MeV and different penetration depth (MFP). As shown, all investigated canister coatings of MAX-phase materials are close in their exposure buildup at all MFP. At low MFP, Ti_3SiC_2 canister coating shows the lowest exposure buildup factor while at high MFP, Ti_2AlC coating shows the lowest buildup values.

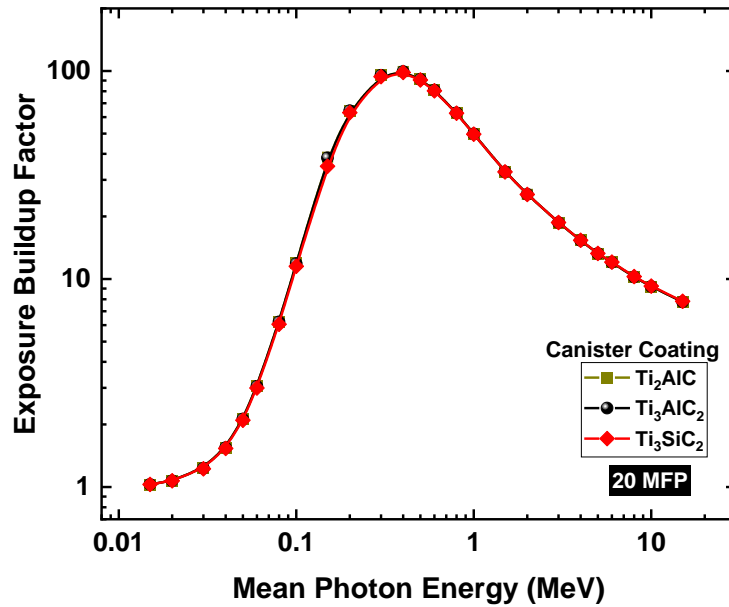


Fig.10. Variation of exposure buildup factor vs. photon energy at 20 MFP for different MAX-phases.

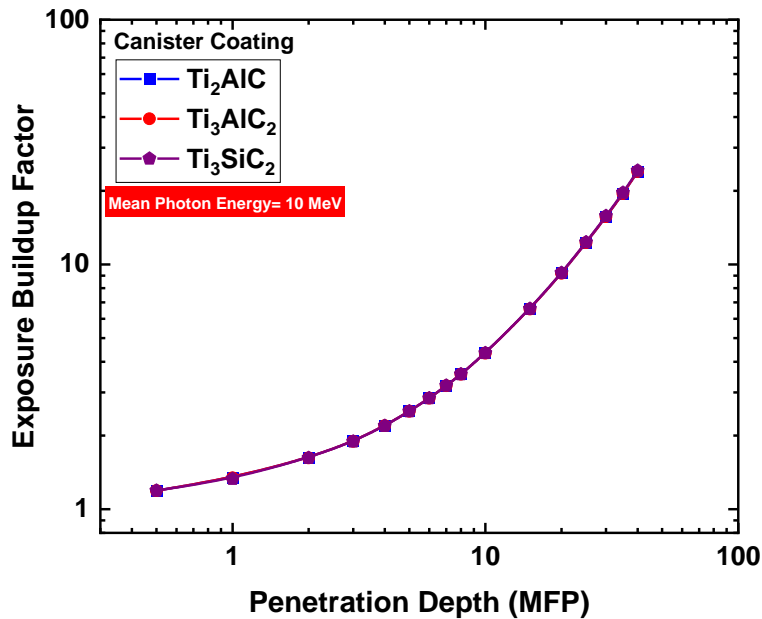


Fig. 11. Variation of exposure buildup factor vs. penetration depth (MFP) at 10 MeV photon energy for different MAX-phases.

IV. Conclusions

The shielding properties of some of the most common MAX-phase materials is investigated as new canister coatings in spent fuel dry storage casks. MicroShield® software package modeled the dry cask consists of three layers, an inner layer of the Alloy 709 canister, an intermediate shielding coating of MAX-phase material and an outer shielding layer of concrete overpack known as ‘Concrete 6’. It was concluded that Ti_3SiC_2 exhibited the highest attenuation coefficients, lowest HVL and MFP values due to its high density of 4.5 g/cm^3 and its silicon (Si) content, which has a higher molar mass (28.0855 g/mol) than aluminum (Al) (26.9815 g/mol). On the other hand, Ti_2AlC showed the highest rate of exposure to gamma radiation at 1.5 MeV while Ti_3SiC_2 showed the lowest rate. Among all MAX-phases investigated, Ti_3SiC_2 canister coating exhibited the lowest values of exposure buildup at photon energies ranging from 0.015 – 2.0 MeV, while Ti_2AlC and Ti_3AlC_2 coatings exhibited the lowest buildup values at energies ranging from 3 – 15 MeV.

Acknowledgments

Work supported by the Russell Family Foundation Grant for research on High Level Waste Packages and Dry Casks, and additional support from the Department of Nuclear Engineering at North Carolina State University.

Conflict of Interest

None.

References

- [1]. Zeinab Y. Alsmadi, Mohamed A. Bourham, "Shielding and corrosion properties of the Alloy 709 as canister material for spent nuclear fuel dry casks", *Defense Technology*, 2022, <https://doi.org/10.1016/j.dt.2022.08.002>.
- [2]. Zeinab Y. Alsmadi, Mohamed Bourham, "Shielding Properties of Alloy 709 Advanced Austenitic Stainless Steel as Candidate Canister Material in Spent Fuel Dry Casks", *International Journal of Physics and Research*, vol. 10, Issue. 2, pp. 11-26 (2020).
- [3]. Muhammad Arif Sazali, Nahrul Khair Alang Md Rashid and Khaidzir Hamzah, "A Review on Multilayer Radiation Shielding", 2019 IOP Conf. Ser.: Mater. Sci. Eng. 555 012008.
- [4]. Youstra Hayouni, Wissem Gallala, Mohamed Essghaier Gaied, Johann Plank, Mohamed Bourham and Zeinab Alsmadi, "Enhanced Shielding and Mechanical Properties of White Cement Mortars via Celestobarite Fine Aggregate", *International Journal of General Engineering and Technology*, vol. 10, Issue. 3, pp. 1-16, May 31st (2021).
- [5]. Zeinab Y. Alsmadi, Mohamed A. Bourham, "Shielding Properties of 316 Stainless Steel with Multi-layered barriers for Spent Fuel Drycasks", *International Journal of Physics and Research*, vol. 11, Issue. 1, pp. 5-20, June 30th (2021).
- [6]. El-Sayed A. Waly, Michael A. Fusco and Mohamed A. Bourham, "Impact of specialty glass and concrete on gamma shielding in multi-layered PWR dry casks", *Progress in Nuclear Energy*, Volume 94, 2017, Pages 64-70.
- [7]. Samah Radwan, Leigh Winfrey and Mohamed Bourham, "Simulation of Particle Impact on Protective Coating of High-Level Waste Storage Packages", *Progress in Nuclear Energy*, vol. 81, pp. 196-202, May 2015.
- [8]. Michael A. Fusco, Leigh Winfrey and Mohamed A. Bourham, "Shielding Properties of Protective Thin Film coatings and Blended Concrete Compositions for High Level Waste Storage Packages", *Annals of Nuclear Energy*, vol. 89, pp. 63-69, March 2016.
- [9]. Zeinab Y. Alsmadi, Mohamed A. Bourham, "An assessment of protective coating dry cask canisters with structurally amorphous metals (SAMs) for enhanced radiation shielding," *Nuclear Engineering and Design*, vol. 388, 2022, 111647.
- [10]. M.I. Sayyed, Kawa M. Kakyb, M.H.A. Mharebd, Alyaa H. Abdalsalam, Nouf Almousa, Ghada Shkoukani and Mohamed A. Bourham, "Borate multicomponent of bismuth rich glasses for gamma radiation shielding application", *Radiation Physics and Chemistry*, Volume 161, 2019, Pages 77-82.
- [11]. Blink, J., Farmer, J., Choi, J. and Saw C., "Applications in the Nuclear Industry for Thermal Spray Amorphous Metal and Ceramic Coatings", *Metall Mater Trans A* 40, 1344-1354 (2009).
- [12]. M. Barsoum, "MAX Phases: Properties of Machinable Ternary Carbides and Nitrides", Wiley-VCH Verlag GmbH & Co. 2013.
- [13]. Barsoum, Michel & Radovic, Miladin. "Mechanical Properties of the MAX Phases." *Annual Review of Materials Research*. 41. 195-227. 2011.
- [14]. M.W. Barsoum, M. Radovic, "Elastic and mechanical properties of the MAX phases", *Annu. Rev. Mater. Res.* 41, pp. 195-227(2011).
- [15]. Maxim Sokol, Varun Natu, Sankalp Kota and Michel W. Barsoum, "On the Chemical Diversity of the MAX Phases", *Trends in Chemistry*, Volume 1, Issue 2, 2019, Pages 210-223.
- [16]. L. Chlubny, J. Lis, K. Chabior, P. Chachlowska, and C. Kapusta, "Processing and Properties of MAX Phases – Based Materials Using SHS Technique" *Archives of Metallurgy and Materials*, vol. 60, no. 2 (2015).
- [17]. G.W. Bentzel, M. Sokol, J. Griggs, A.C. Lang and M.W. Barsoum, "On the interactions of Ti₂AlC, Ti₃AlC₂, Ti₃SiC₂ and Cr₂AlC with palladium at 900 °C", *Journal of Alloys and Compounds*, Volume 771, 2019, Pages 1103-1110.
- [18]. Zeinab Y. Alsmadi, Abdullah Alomari, N. Kumar, K.L. Murty, "Effect of Hold Time on High Temperature Creep-Fatigue Behavior of Fe-25Ni-20Cr (wt.%) Austenitic Stainless Steel (Alloy 709)", *Material Science and Engineering: A*, vol. 771, pp. 138591 (2020).
- [19]. Zeinab Y. Alsmadi, K.L. Murty, "Effect of Strain Range on High Temperature Creep-Fatigue Behavior of Fe-25Ni-20Cr (wt.%) Austenitic Stainless Steel (Alloy 709)", *Materials at High Temperatures*, December 19th (2020). DOI: 10.1080/09603409.2020.1859310.
- [20]. Zeinab Y. Alsmadi, K.L. Murty, "High-temperature effects on creep-fatigue interaction of the Alloy 709 austenitic stainless steel", *International Journal of Fatigue*, vol. 143, 105987 (2021).
- [21]. D.J. Tallman, M. Naguib, B. Anasori and M.W. Barsoum, "Tensile creep of Ti₂AlC in air in the temperature range 1000-1150 °C", *Scr. Mater.* 66 (2012) 805-808.
- [22]. M. Radovic, M.W. Barsoum, T. El-Raghy and S. Wiederhorn, "Tensile creep of fin grained (3-5 μm) Ti₃SiC₂ in the 1000-1200 °C temperature range", *Acta Mater.* 49 (2001) 4103-4112.
- [23]. M. Radovic, M.W. Barsoum, T. El-Raghy and S.M. Wiederhorn, "Tensile creep of coarse-grained Ti₃SiC₂ in the 1000-1200 °C temperature range", *J. Alloys Compd.* 361 (2003) 299-312.
- [24]. T. Zhen, M.W. Barsoum, S.R. Kalidindi, M. Radovic, Z.M. Sun and T. El-Raghy, "Compressive creep fine and coarse-grained Ti₃SiC₂ in air in the 1100-1300 °C temperature range", *Acta Mater.* 53 (2005) 4963-4973.
- [25]. T.A. Prikhna, S.N. Dub, A.V. Starostina, M.V. Karpets, T. Cbiosh and P. Chartier, "Mechanical properties of materials based on MAX phases of the Ti-Al-C system", *J. Superhard Mater.* 34 (2012) 102-109.
- [26]. M.W. Barsoum, T. El-Raghy and L. Ogbuji, "Oxidation of Ti₃SiC₂ in air", *J. Electrochem. Soc.* 144 (1997) 2508-2516.
- [27]. S.B. Li, X.D. Chen, Y. Zhou and G.M. Song, "Influence of grain size on high temperature oxidation behavior of Cr₂AlC ceramics", *Ceram. Int.* 39 (2013) 2715-2721.
- [28]. X.H. Wang, Y.C. Zhou, "Layered machinable and electrically conductive Ti₂AlC and Ti₃AlC₂ ceramics: a review", *J. Mater. Sci. Tech.* 26 (2010) 385-416.
- [29]. M. Sundberg, G. Malmqvist, A. Magnusson and T. El-Raghy, "Alumina forming high temperature silicides and carbides", *Ceram. Int.* 30 (2004) 1899-1904.
- [30]. S. Li, G. Song, K. Kwakernaak, S. vand der Zwaag and W.G. Sloof, "Multiple crack healing of a Ti₂AlC ceramic", *J. Eur. Ceram. Soc.* 32 (2012) 1813-1820.
- [31]. Alsmadi, Z.Y.; Abouelella, H.; Alomari, A.S.; Murty, K.L, "Stress-Controlled Creep-Fatigue of an Advanced Austenitic Stainless Steel at Elevated Temperatures", *Materials* 2022, Volume 15, 3984, <https://doi.org/10.3390/ma15113984>.

- [32]. M. Radovic, M.W. Barsoum, "MAX phases: Bridging the gap between metals and ceramics", *Am. Ceram. Soc. Bull.* 92 (2013) 20–27.
- [33]. M.W. Barsoum, "Physical properties of MAX phases", in K.H.J. Buschow, R.W. Cahn, M.C. Flemings, E.J. Kramer, S. Mahajan, and P. Veysiere (Ed.), *Encyclopedia of Materials* 2006, Elsevier (2006).
- [34]. El-Sayed A. Waly, Mohamed A. Bourham, "Comparative study of different concrete composition as gamma-ray shielding materials", *Annals of Nuclear Energy*, Volume 85, 2015, Pages 306-310.
- [35]. Naegeli, R.E., (2004), "Calculation of Radionuclides in PWR Spent Fuel Samples for SFR Experiment Planning". Sandia National Laboratories.
- [36]. MicroShield®, Grove Software, <http://radiationsoftware.com/microshield/>.
- [37]. U.S. Nuclear Regulatory Commission. (2002). *Radioactive Waste: Production, Storage Disposal*. NUREG/BR-0216, Rev. 2.
- [38]. U.S. Nuclear Regulatory Commission, (2015). Typical dry cask storage system. Retrieved from (<http://www.nrc.gov/waste/spent-fuel-storage/diagramtypical-dry-casksystem.html>).
- [39]. Weiner, Ruth F., Osborn, Douglas., and Marincel, Michelle K., "Microshield Analysis to Calculate External Radiation Dose Rates for Several Spent Fuel Casks". United States: N. p., 2007. <https://www.osti.gov/servlets/purl/1267224>.
- [40]. Irsyad, Sigit Purnomo, Rini Heroe Oetami, "Design of reflector {TRIGA} mark {II} Bandung waste container shielding using micro shield 7.02.". *Journal of Physics: Conference Series*. Vol. 1436, N.1, p. 012076. 2020. DOI: 10.1088/1742-6596/1436/1/012076.
- [41]. Kim, Jong Hoa, Jeon, Homin, Kim, Yong Sik, Han, Kyeong Ho, & Seo, Jang Soo (2017). "Estimation of mixed nuclide inventory using microshield computer program". *Proceedings of the Conference and Symposium Korean Radioactive Waste Society Spring Meeting 2017*, (p. 420). Korea, Republic of: KRS.
- [42]. El-Sayed A. Waly, Michael A. Fusco and Mohamed A. Bourham, "Gamma-ray mass attenuation coefficient and half value layer factor of some oxide glass shielding materials", *Annals of Nuclear Energy*, Volume 96, 2016, Pages 26-30.
- [43]. Kaundal RS, Kaur S, Singh N, Singh KJ, "Investigation of structural properties of lead strontium borate glasses for gamma-ray shielding applications". *J. Phys. Chem. Solids* 71, 1191-1195(2010).